


Nodal Line Spin-Gapless Semimetals and High-Quality Candidate Materials

Run-Wu Zhang,[‡] Zeying Zhang,[‡] Cheng-Cheng Liu,^{*} and Yugui Yao[†]

Key Lab of Advanced Optoelectronic Quantum Architecture and Measurement (MOE), Beijing Key Lab of Nanophotonics, and Ultrafine Optoelectronic Systems, and School of Physics, Beijing Institute of Technology, Beijing 100081, China

 (Received 28 June 2019; published 10 January 2020)

Spin-gapless semimetals (SGSMs), which generate 100% spin polarization, are viewed as promising semi-half-metals in spintronics with high speed and low consumption. We propose and characterize a new Z_2 class of topological nodal line (TNL) in SGSMs. The proposed TNLSGSMs are protected by space-time inversion symmetry or glide mirror symmetry with two-dimensional (2D) fully spin-polarized nearly flat surface states. Based on first-principles calculations and effective model analysis, a series of high-quality materials with $R\bar{3}c$ and $R3c$ space groups are predicted to realize such TNLSGSMs (chainlike). The 2D fully spin-polarized nearly flat surface states may provide a route to achieving equal spin pairing topological superconductivity as well as topological catalysts.

DOI: 10.1103/PhysRevLett.124.016402

Introduction.—Spintronics, using an electron's spin instead of its charge to carry information and featuring high speed and low energy consumption, has attracted tremendous interest from academic research to industrial applications in recent years [1,2]. Half-metals manifest one spin channel possessing metallic states while the other keeps insulating or semiconducting. Unlike conventional ferromagnetic (FM) alloys with a low degree of spin polarization, half-metals with 100% spin polarization are regarded as excellent spintronics candidates for spin generation, injection, and transport. Recently, as a remarkable upgraded version of half-metals, spin-gapless semiconductors (SGSs) had been proposed [3]. In addition to the advantages of standard half-metals, SGSs have large electron mobility and highly tunable capabilities using external fields, such as pressure, electric fields, magnetic fields, electromagnetic radiation, etc. The unique SGSs provide a new playground and opportunities for spintronics, electronics, and optics. In particular, the SGSs own ideal Weyl points for the metallic spin channel without other entangled trivial bands, which marry spintronics and topological physics.

Topological semimetals (TSMs) are systems where the conduction and valence bands cross each other with robustness in the Brillouin zone (BZ). Among TSMs, topological nodal line semimetals (TNLSs) are regarded as a new class of topological quantum states [4–30], which bridge the gapped and gapless phases, can be driven into various topological phases, such as topological insulators and Dirac (Weyl) semimetals [31–45]. In particular, important works on topological half-metals [46,47] have attracted an enormous amount of attention due to potential applications in spintronics. Many intriguing physical properties have been proposed in these interesting TNLSs, including Friedel oscillation [13], nondispersive Landau

energy level [48], specific long-range Coulomb interactions [49], etc.

Buoyed by the aforementioned superior properties, the efficient combination of the spin-gapless feature and a TNLS nature is desirable. In this Letter, we first showcase a general classification of TNL spin-gapless semimetals (SGSMs) and further propose an enhanced NL connection mode (dubbed a nodal chain SGSM). The coexistence of spin-polarized and linear dispersion in the NL states can be realized in a family of real materials with $R\bar{3}c$ and $R3c$ space groups. These ideal candidates feature ultraclean energy dispersion and ultrahigh Fermi velocity, which vastly enriches the TNLS and half-metal family. Distinguished from most proposed nodal chain states, the fourfold degeneracy neck crossing point traces out twofold degeneracy lines emerged in the single spin channel, and the profile of nodal chainlike SGSMs are revealed by the tight-binding (TB) model. The efficient combination of a nodal chain and a fully spin-polarized nature in feasible materials greatly refreshes thinking for the design of potential high-performance spintronic devices.

Nodal line spin-gapless semimetal.—According to the different spin-polarized band crossing patterns at the Fermi level, NLSGSMs could give rise to two possible configurations. Here, we construct a two-band model for describing the classifications of NLSGSMs. We consider an effective Hamiltonian near Γ ,

$$H(k) = [(\cos k_x + \cos k_y - r_s)\sigma_1 + \sin k_z \sigma_3]s_3 + m(1 - s_3)\sigma_2, \quad (1)$$

where the Pauli matrices $\sigma_{i=1,2,3}$ label the orbital degree of freedom, $s_3 = 1(-1)$ represents the spin-up (spin-down)

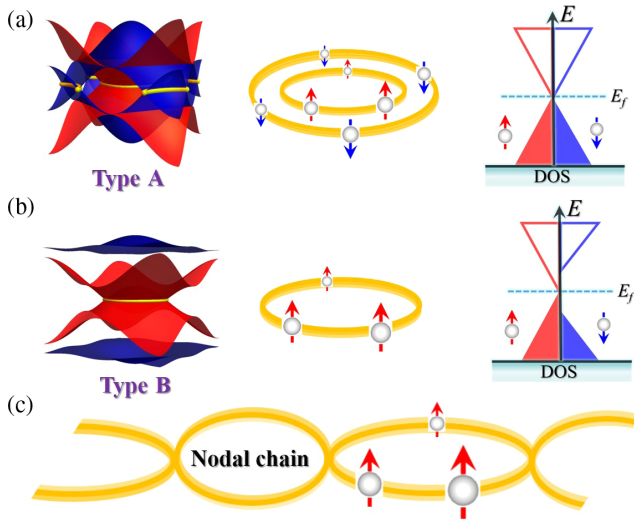


FIG. 1. Schematic illustration of the simplest TNLSGSMs between two inverted subbands and the corresponding density of states (DOS) for (a) concentric loops that come from different spin channels separately, and (b) NLs that come from a single spin channel. (c) Schematic figure showing nodal chain SGSMs consisting of TNLSGSMs. The red (blue) pattern represents the spin-up (spin-down) channel.

component, and $r_s = 2 - s_3$ stands for the radius of nodal lines. We first put forward a general framework to classify two kinds of NLSGSMs (Fig. 1) and tabulate the corresponding effective Hamiltonians and the connection modes of NLSGSMs in Table I. Regarding type-A NLSGSMs [Fig. 1(a)], opposite spin-polarized states coexist at the Fermi level, which greatly decreases the pure spin-polarized current. Moreover, the hybrid spin current would restrict the further practicability of NLSGSMs. By comparison, type-B NLSGSMs, as pictured in Fig. 1(b), which can effectively avoid the shortcomings of the coexistence of the two spin channel currents, which are the focus of our Letter.

Compared to Weyl or Dirac semimetal with monotonic structural variations, the TNL family can exhibit numerous cross-connection configurations in momentum space, including nodal lines [4–20], nodal chains [21,22], nodal links [23,24], nodal nets [25–28], and nodal knots [29,30], which will provide more candidates for high-performance spintronic materials. The drumheadlike surface states as a significant indicator of TNLSs, may generate exotic behavior [13,48,49]. It is desirable to search for large

TABLE I. Parameters of effective models in two kinds of NLSGSMs.

Classification	$s_3 = 1$	$s_3 = -1$	Description
	(spin up)	(spin down)	
Type A		$m = 0$	Fig. 1(a)
Type B		$m \neq 0$	Fig. 1(b)

drumheadlike surface states in SGSMs. Via different cross-connection modes, multiple NLSGSMs (e.g., nodal chain SGSMs), as pictured in Fig. 1(c), can produce a larger surface density of states compared to a single NL, which may offer an effective avenue to study more interesting effects.

High-quality candidate materials.—The concrete materials realization plays an important role in turning the theoretical prototypes into reality. Here, we sort out a series of candidates with NLSGSM (chainlike) states that have not been mentioned to date, involving rhombohedral transition metal trifluorides with an $R\bar{3}c$ space group (i.e., PdF₃ [50] and MnF₃ [51]) and rhombohedral transition metal carbonates (or borates) with an $R\bar{3}c$ space group [i.e., FeCO₃ (Siderite) [52], TiBO₃ [53], MnBO₃, LaMnO₃ [54], and LaNiO₃ [55] as well as rhombohedral transition metal phosphates with an $R\bar{3}c$ space group [i.e., XTiMn(PO₄)₃, X = Ca, Mg, Zn], as shown in Figs. 2(a)–2(c), respectively. In these nodal chain SGSMs, they are characterized by ultraclean energy dispersion and ultrahigh Fermi velocity, which will vastly promote the experimental progress of NLSGSMs family. We will focus on two representative candidates from the two distinct space groups, i.e., PdF₃ and ZnTiMn(PO₄)₃, and further understand the striking physics for the nodal chain SGSMs. Moreover, the remaining candidates with very similar electronic features are provided in Ref. [56].

As an ideal nodal chain SGSM candidate, PdF₃ was first identified with powder x-ray diffraction in 1957 [50] and shares an $R\bar{3}c$ (D_{3d}^6 , no. 167) space group with a rhombohedral primitive unit cell composed of eight atoms. The optimized lattice constants for PdF₃ agree well with the experimental lattice parameters [50], and the computational details are shown in Table S11 of the Supplemental Material (SM) [56]. Also, we further screen nodal chain SGSM candidates [e.g., XTiMn(PO₄)₃, X = Ca, Mg, Zn] in a similar $R\bar{3}c$ space group (C_{3v}^6 , no. 161) from the Materials Project [68]. These transition metal phosphates pave the way to design novel nodal chain SGSM materials. Regarding the transition metal-based materials, the magnetic property is generally attributed to the transition metal atoms. To determine the magnetic ground states of PdF₃ and ZnTiMn(PO₄)₃, we calculate the total energies of three different magnetic configurations, including FM and two antiferromagnetic (AFM1 and AFM2) configurations, as shown in Fig. S1 of the SM [56]. We find that the FM state is lower in energy than the AFM1 and AFM2 states, respectively, indicating that PdF₃ and ZnTiMn(PO₄)₃ prefer FM ground states (see the details in Table S12 of the SM [56]).

Stable FM ground states provide us with the motivation to further explore the desired properties for PdF₃ and ZnTiMn(PO₄)₃. In Figs. 2(d) and 2(e), both of the band structures show a linear dispersion semimetallic feature in the spin-up channel, whereas the spin-down channel

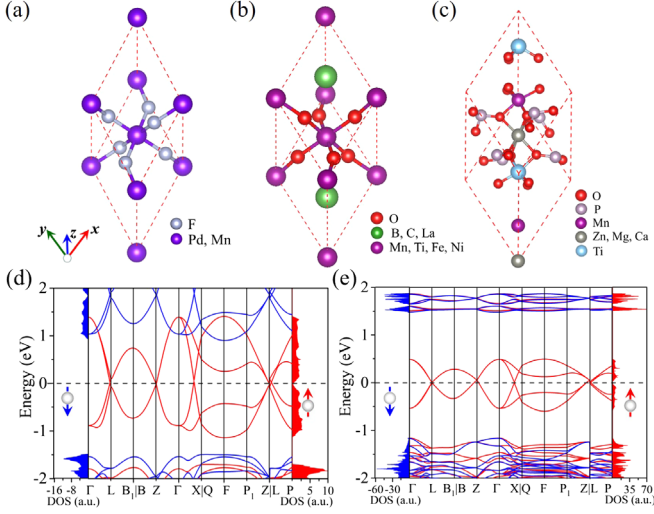


FIG. 2. (a) The primitive unit cell with a nonsymmorphic $R\bar{3}c$ rhombohedral lattice of TMF_3 (TM = Mn, Pd) and (b) ABO_3 -type perovskites (i.e., FeCO_3 , MnBO_3 , TiBO_3 , LaMnO_3 , and LaNiO_3). (c) The primitive unit cell with $R3c$ rhombohedral $A'\text{ABO}_3$ -type perovskites [i.e., $\text{XTiMn}(\text{PO}_4)_3$; X = Ca, Mg, Zn]. Spin-resolved band structures and DOS of (d) PdF_3 and (e) $\text{ZnTiMn}(\text{PO}_4)_3$ ($U = 4$ eV). The red and blue lines represent spin-up and spin-down channels, respectively.

presents a semiconductor with large gaps of 2.39 and 2.64 eV. Indeed, from the density of states (DOS) in PdF_3 and $\text{ZnTiMn}(\text{PO}_4)_3$, the energy ranges of linear dispersion are enough to overcome the interruption of irrelevant bands, therefore making ideal half-metals with a fully spin-polarized nature. Generally, the bigger slope is expected to be of higher Fermi velocity in the linear dispersion system. As for PdF_3 and $\text{ZnTiMn}(\text{PO}_4)_3$, the Fermi velocities are estimated at about 4.85×10^5 and 2.98×10^5 m/s, respectively, along the $\Gamma \rightarrow X$ path, which is on the order of graphene, meaning that these candidates would possess more intriguing properties.

As for the $R\bar{3}c$ space group (e.g., PdF_3), the symmetries include the following important operations: the space-inversion symmetry \mathcal{P} , the threefold rotation \mathcal{C}_3 along the [111] direction, and the glide mirrors ($\tilde{\mathcal{M}}_{x-y}$, $\tilde{\mathcal{M}}_{y-z}$, $\tilde{\mathcal{M}}_{-xz}$). In $\text{ZnTiMn}(\text{PO}_4)_3$, the Ti and Mn sites are inequivalent, leaving \mathcal{P} broken, the $R\bar{3}c$ transforms into the $R3c$, then the operations reduce to the \mathcal{C}_3 and the three glide mirrors only. In Figs. 2(d) and 2(e), the crossing node Z appears at both the PdF_3 and the $\text{ZnTiMn}(\text{PO}_4)_3$, which is a noticeable feature in the linear dispersion band structures. To trace this trait, our further analysis shows that the two-dimensional irreducible real representation of \mathcal{C}_3 symmetry based on d_{yz} and d_{xz} generates two pairs of twofold degeneracy [69]. Moreover, the Z point is the invariant point of the rotation part of three glide mirrors, and the nonsymmorphic symmetry $\tilde{\mathcal{C}}_{2(x-y)}$ or $\tilde{\mathcal{M}}_{x-y}$ constrains the Hamiltonian and leads to another pair of twofold degeneracy at the Z point [70]. Remarkably, the former

twofold degeneracy is from the symmorphic symmetry (the same atom's d orbitals), and the latter twofold degeneracy is from the nonsymmorphic symmetry (different atom's d orbitals). Therefore, the neck crossing point Z features fourfold degeneracy.

From the orbital projection analysis, as plotted in Fig. S2 of the SM [56], the low-energy dispersion of the spin-up channel near the Fermi level is mainly dominated by the $4d$ ($3d$) orbitals of Pd (Mn) atoms. PdF_3 and $\text{ZnTiMn}(\text{PO}_4)_3$ manifest the triangular twisted oxygen octahedral crystal feature, which induces Pd (Mn) d orbitals to split into two groups: A_{1g} (d_{z^2}) and E_g $\{(d_{x^2-y^2}, d_{xy}), (d_{xz}, d_{yz})\}$ in the $R\bar{3}c$ and the $R3c$ space groups. Considering the correlation effects for transition metal elements in PdF_3 and $\text{ZnTiMn}(\text{PO}_4)_3$, wide range Hubbard U values (3–5 eV) are checked in Fig. S3 of the SM [56]. We can see that the obvious character of the SGSMs are robust against the various U values.

In the spin-polarized system, spin is a good quantum number, and degrees of freedoms of the spin and the orbital are independent; therefore the crystalline symmetries for the single spin channel can be preserved [47]. To better capture the key physics underlying nodal chain SGSMs, we develop a TB model by considering d-d hoppings using the minimal set of d_{xz} and d_{yz} orbitals as bases. To conveniently describe the atomic bases via the $R\bar{3}c$ and the $R3c$ space groups, we denote them as $\varphi_1 = |d_{xz}\rangle$ and $\varphi_2 = |d_{yz}\rangle$, and considering the nearest-neighbor and the next-nearest-neighbor hoppings, the TB model Hamiltonian can be expressed as

$$H_{lm'l'}(\mathbf{k}) = \sum_{\mathbf{d}_j} e^{i\mathbf{k}\cdot\mathbf{d}_j} E_{lm'l'}(\mathbf{d}_j),$$

$$E_{lm,l'm'}(\mathbf{d}_j) = \langle \varphi_m(\mathbf{r} - \mathbf{d}_l) | H | \varphi_{m'}(\mathbf{r} - \mathbf{d}_{l'} - \mathbf{R}_j) \rangle, \quad (2)$$

where l is the atom index, $E_{lm'l'}(\mathbf{d}_j)$ denotes the hopping integrals for neighboring sites with displacement \mathbf{d}_j . The hopping integrals to $R\mathbf{d}_j$ sites can be generated by \mathbf{d}_j [57,71],

$$E_{\bar{l}m\bar{l}m'}(R\mathbf{d}_j) = D(R)E_{lm'l'}(\mathbf{d}_j)[D(R)]^\dagger, \quad (3)$$

where R is the rotation part of symmetry operator, $\mathbf{d}_i = \{R|\mathbf{t}\}\mathbf{d}_l$, and $D(R)$ is the representation matrix of the E_g irreducible representation. The detailed Hamiltonians of PdF_3 and $\text{ZnTiMn}(\text{PO}_4)_3$ are given in the Model Section of the SM [56]. The band structures calculated by the TB model Hamiltonian agree well with the ones obtained by the density functional theory (DFT) method in the whole BZ, as shown in Figs. 3(a) and 3(b). Interestingly, the spin-resolved band structures of PdF_3 [Fig. 3(a)] and $\text{ZnTiMn}(\text{PO}_4)_3$ [Fig. 3(b)] are similar, except that $\text{ZnTiMn}(\text{PO}_4)_3$ has a tiny gap along the $\Gamma \rightarrow X$ path due to the fact that \mathcal{P} is broken.

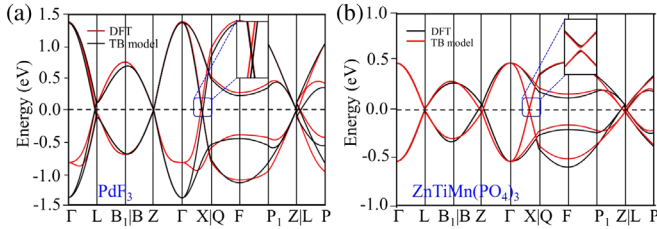


FIG. 3. The band structures of DFT (black solid curves) agree with that of the effective lattice model (red solid curves) calculations in (a) PdF₃ and (b) ZnTiMn(PO₄)₃ systems.

The evolution of crossing nodes develops two kinds of cross-connection modes under the $R\bar{3}c$ constraint, i.e., nodal chains and NLs. In PdF₃, the profile of all nodes is revealed by the TB model clearly, as shown in Figs. 4(a) and 4(b). For case I, the cross-connection structure [see Fig. 4(b)] with three NLs (i.e., NL1, NL2, and NL3) are pinned at the Z point to form a nodal chainlike structure. The neck crossing point Z is coconstrained by the C_3 rotation symmetry along the $\Gamma - Z$ high symmetry line and the nonsymmorphic symmetry $\tilde{C}_{2(x-y)}$ or \tilde{M}_{x-y} . Remarkably, the NL1 on the glide mirror \tilde{M}_{y-z} plane is just accidentally formed rather than protected by the nonsymmorphic symmetry (see Fig. S4 of the SM [56]).

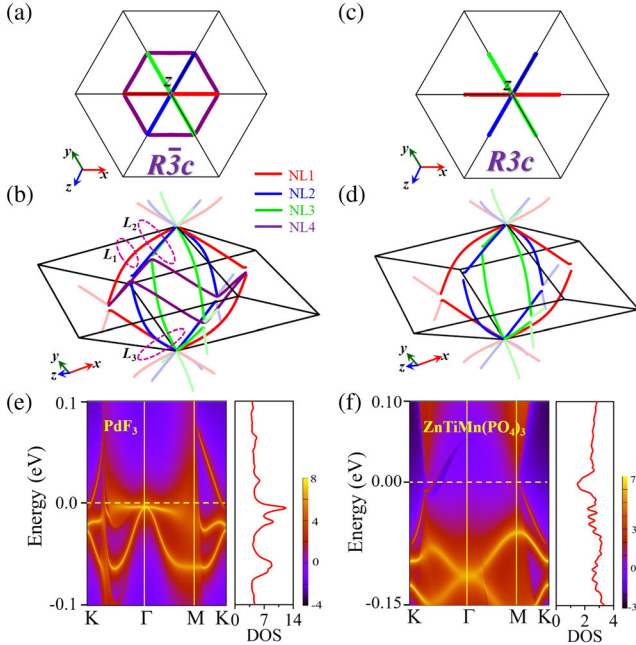


FIG. 4. (a)–(d) The profile of the nodal chainlike SGSMs in three-dimensional k space, including the top views (a) PdF₃ and (c) ZnTiMn(PO₄)₃ along the [111] direction, the side views (b) PdF₃ and (d) ZnTiMn(PO₄)₃. Different colors (i.e., the red, blue, green, and purple lines) correspond to different orientations of the NLs (i.e., NL1, NL2, NL3, and NL4). Band structures and DOSs for surface (111) and in (e) PdF₃ and (f) ZnTiMn(PO₄)₃. The purple dashed lines labeled L_1 , L_2 , and L_3 represent three respective loops along which the Berry phase is calculated.

In combination with \tilde{M}_{y-z} and C_3 rotation symmetries, NL2 and NL3 possess the same characteristics. Besides, as seen in Fig. 4(b), akin to alkaline-earth compounds [58], the case-II cross-connection structure (i.e., NL4) is protected by \mathcal{P} and the complex conjugate operator \mathcal{K} . Meanwhile, the “snakelike” NL4 can be annihilated in ZnTiMn(PO₄)₃ since \mathcal{P} disappears, as displayed in Figs. 4(c) and 4(d). The topological protection of NL1 (NL2 or NL3 or NL4) is further checked by directly calculating the nontrivial π Berry phase along a small loop (L_1) enclosing the NL. Moreover, based on L_2 (or L_3) encircling the number of the nodal chain (two NLs or three NLs), zero (or π) Berry phase is obtained. As a result, the origin of multiple lines (nodal chain and NL) is revealed, and a detailed analysis is given in the Model Section of the SM [56].

Discussion.—We further investigated the robustness and the feasibility of nodal chainlike SGSMs. Taking PdF₃ as an example, we impose a small perturbation (e.g. external triaxial strain) on it. Compared with the fragile NLSs, the band structures of PdF₃ under such a wide range of triaxial compressional strains (0%–10%), all crossing nodes still exist as expected, manifesting the robustness of a Weyl nodal chain against certain structural deformation (see the details in Fig. S5 of the SM [56]).

Practically, as an essential property of magnetic material PdF₃, magnetic anisotropy has a great significance for aligning the magnetic moments in magnetic storage media. To further determine the magnetocrystalline anisotropy energy (MAE) of PdF₃, we calculate the angular dependence of the MAE on the magnetization angle θ as a function of polar angles in different directions on the $x(y)$ - z and x - y planes, as plotted in Fig. S6 of the SM [56]. It is obvious that MAE is nearly equivalent to the ϕ evolution in the x - y plane. Regarding the $x(y)$ - z plane, the MAE of PdF₃ can reach the maximal value 1.19 meV/atom at the $\theta = 0$ (deg), which is 1 order of magnitude larger than that of the MAE in cubic Fe, Co, and Ni [72], meaning that PdF₃ prefers the FM state with the spin aligned along the z direction in the conventional cell (i.e., the [111] in the unit cell).

The hallmark drumhead surface states for topological NLSGSMs PdF₃ and ZnTiMn(PO₄)₃ are shown in Figs. 4(e) and 4(f). Owing to the lack of chiral symmetry or particle-hole symmetry in real solid materials, the drumhead states are dispersive indeed, and the dispersion strength is material dependent. The peaklike DOSs from the nearly flat drumhead states are clearly shown for PdF₃, as plotted in Fig. 4(e). Volovik and co-workers proposed that 2D flatbands with large DOSs provide a route to achieving high-temperature superconductivity [73–75]. Besides, recent experimental and theoretical advances [46,47,76–81] in the nodal half-metal states offered a tremendous boost to the emerging field of the magnetic semimetal’s community. Herein, we would like to stress

that the 2D nearly flat drumhead states in TNLSGSMs not only have large DOSs but also are fully spin polarized. Such fully spin-polarized nearly flat drumhead states would lead to the equal spin pairing topological superconductivity, such as p or f wave topological superconductivity, which supports Majorana zero bound states at vortices with non-Abelian statistics for the intriguing proposal of topological quantum computation. Recently, topological catalysts provide a potential platform to create active sites [82–84]. PdF₃ as a Pd-based noble metal binary compound, which would be a better electrocatalyst for the hydrogen evolution reaction due to the following distinguishing aspects: (i) Pd itself is a good catalyst, (ii) topological nodal chain induced large drumhead surface states can offer sufficient active planes, and (iii) SGSM featured linear crossings of energy bands can provide high carrier mobility near Fermi level. Therefore, PdF₃ showcases a new routine to design a promising electrocatalyst.

Conclusion.—In this Letter, we first introduce a general framework to classify opposite and same spin-polarized Weyl nodal chainlike states in SGSMs, and we propose a series of realistic materials to realize hitherto unreported fully spin-polarized nodal chain states. These high-quality materials harbor ultraclean energy dispersion and ultrahigh Fermi velocity, which is rather robust against strong triaxial compressional strain. The proposal of TNLSGSMs and their materials realization greatly expands the TSM family and provides a good playground for spintronics, topological superconductivity, and topological catalysts.

The work is supported by the National Natural Science Foundation of China (Grants No. 11734003, No. 11922401, No. 11774028, and No. 11574029), the National Key R&D Program of China (Grant No. 2016YFA0300600), the Strategic Priority Research Program of Chinese Academy of Sciences (Grant No. XDB30000000), and Basic Research Funds of Beijing Institute of Technology (Grant No. 2017CX01018). R.-W.Z. also thanks the Graduate Technological Innovation Project of the Beijing Institute of Technology (Grants No. 2018CX10028 and No. 2019CX10018) for the support.

*ccliu@bit.edu.cn

†ygyao@bit.edu.cn

‡These authors contributed equally to this work.

- [1] S. A. Wolf, D. D. Awschalom, R. A. Buhrman, J. M. Daughton, S. von Molnár, M. L. Roukes, A. Y. Chtchelkanova, and D. M. Treger, *Science* **294**, 1488 (2001).
- [2] I. Žutić, J. Fabian, and S. D. Sarma, *Rev. Mod. Phys.* **76**, 323 (2004).
- [3] X. Wang, *Phys. Rev. Lett.* **100**, 156404 (2008).
- [4] K. Mullen, B. Uchoa, and D. T. Glatzhofer, *Phys. Rev. Lett.* **115**, 026403 (2015).
- [5] C. Fang, Y. Chen, H.-Y. Kee, and L. Fu, *Phys. Rev. B* **92**, 081201(R) (2015).

- [6] H. Weng, Y. Liang, Q. Xu, R. Yu, Z. Fang, X. Dai, and Y. Kawazoe, *Phys. Rev. B* **92**, 045108 (2015).
- [7] Y. Kim, B. J. Wieder, C. L. Kane, and A. M. Rappe, *Phys. Rev. Lett.* **115**, 036806 (2015).
- [8] R. Yu, H. Weng, Z. Fang, X. Dai, and X. Hu, *Phys. Rev. Lett.* **115**, 036807 (2015).
- [9] M. Ezawa, *Phys. Rev. Lett.* **116**, 127202 (2016).
- [10] G. Bian, T.-R. Chang, R. Sankar, S.-Y. Xu, H. Zheng, T. Neupert, C.-K. Chiu, S.-M. Huang, G. Chang, I. Belopolski *et al.*, *Nat. Commun.* **7**, 10556 (2016).
- [11] J. Hu, Z. Tang, J. Liu, X. Liu, Y. Zhu, D. Graf, K. Myhro, S. Tran, C. N. Lau, J. Wei *et al.*, *Phys. Rev. Lett.* **117**, 016602 (2016).
- [12] L. M. Schoop, M. N. Ali, C. Straer, A. Topp, A. Varykhalov, D. Marchenko, V. Duppel, S. S. P. Parkin, B. V. Lotsch, and C. R. Ast, *Nat. Commun.* **7**, 11696 (2016).
- [13] R. Li, H. Ma, X. Cheng, S. Wang, D. Li, Z. Zhang, Y. Li, and X.-Q. Chen, *Phys. Rev. Lett.* **117**, 096401 (2016).
- [14] S. Kobayashi, Y. Yamakawa, A. Yamakage, T. Inohara, Y. Okamoto, and Y. Tanaka, *Phys. Rev. B* **95**, 245208 (2017).
- [15] Y. Sun, Y. Zhang, C.-X. Liu, C. Felser, and B. Yan, *Phys. Rev. B* **95**, 235104 (2017).
- [16] S. Li, Z.-M. Yu, Y. Liu, S. Guan, S.-S. Wang, X. Zhang, Y. Yao, and S. A. Yang, *Phys. Rev. B* **96**, 081106(R) (2017).
- [17] J. Wang, *Phys. Rev. B* **96**, 081107(R) (2017).
- [18] R.-W. Zhang, C.-C. Liu, D.-S. Ma, M. Wang, and Y. Yao, *Phys. Rev. B* **98**, 035144 (2018).
- [19] D.-S. Ma, J. Zhou, B. Fu, Z.-M. Yu, C.-C. Liu, and Y. Yao, *Phys. Rev. B* **98**, 201104(R) (2018).
- [20] C. Gong, Y. Xie, Y. Chen, H.-S. Kim, and D. Vanderbilt, *Phys. Rev. Lett.* **120**, 106403 (2018).
- [21] T. Bzdusek, Q. Wu, A. Ruegg, M. Sigrist, A. Soluyanov, *Nature (London)* **538**, 75 (2016).
- [22] S.-S. Wang, Y. Liu, Z.-M. Yu, X.-L. Sheng, and S. A. Yang, *Nat. Commun.* **8**, 1844 (2017).
- [23] Z. Yan, R. Bi, H. Shen, L. Lu, S.-C. Zhang, and Z. Wang, *Phys. Rev. B* **96**, 041103(R) (2017).
- [24] W. Chen, H.-Z. Lu, and J.-M. Hou, *Phys. Rev. B* **96**, 041102 (R) (2017).
- [25] B. Fu, X. Fan, D. Ma, C.-C. Liu, and Y. Yao, *Phys. Rev. B* **98**, 075146 (2018).
- [26] B. Singh, B. Ghosh, C. Su, H. Lin, A. Agarwal, and A. Bansil, *Phys. Rev. Lett.* **121**, 226401 (2018).
- [27] X. Feng, C. Yue, Z. Song, Q. S. Wu, and B. Wen, *Phys. Rev. Mater.* **2**, 014202 (2018).
- [28] J.-T. Wang, S. Nie, H. Weng, Y. Kawazoe, and C. Chen, *Phys. Rev. Lett.* **120**, 026402 (2018).
- [29] M. Ezawa, *Phys. Rev. B* **96**, 041202(R) (2017).
- [30] R. Bi, Z. Yan, L. Lu, and Z. Wang, *Phys. Rev. B* **96**, 201305 (R) (2017).
- [31] C. L. Kane and E. J. Mele, *Phys. Rev. Lett.* **95**, 226801 (2005).
- [32] B. A. Bernevig, T. L. Hughes, and S.-C. Zhang, *Science* **314**, 1757 (2006).
- [33] X. Wan, A. M. Turner, A. Vishwanath, and S. Y. Savrasov, *Phys. Rev. B* **83**, 205101 (2011).
- [34] S. M. Young, S. Zaheer, J. C. Y. Teo, C. L. Kane, E. J. Mele, and A. M. Rappe, *Phys. Rev. Lett.* **108**, 140405 (2012).
- [35] B.-J. Yang and N. Nagaosa, *Nat. Commun.* **5**, 4898 (2014).

- [36] Z. Wang, Y. Sun, X.-Q. Chen, C. Franchini, G. Xu, H. Weng, X. Dai, and Z. Fang, *Phys. Rev. B* **85**, 195320 (2012).
- [37] Z. Wang, H. Weng, Q. Wu, X. Dai, and Z. Fang, *Phys. Rev. B* **88**, 125427 (2013).
- [38] T.-R. Chang, S.-Y. Xu, D. S. Sanchez, W.-F. Tsai, S.-M. Huang, G. Chang, C.-H. Hsu, G. Bian, I. Belopolski, Z.-M. Yu, S. A. Yang, T. Neupert, H.-T. Jeng, H. Lin, and M. Z. Hasan, *Phys. Rev. Lett.* **119**, 026404 (2017).
- [39] G. Xu, H. Weng, Z. Wang, X. Dai, and Z. Fang, *Phys. Rev. Lett.* **107**, 186806 (2011).
- [40] H. Weng, C. Fang, Z. Fang, B. A. Bernevig, and X. Dai, *Phys. Rev. X* **5**, 011029 (2015).
- [41] A. A. Soluyanov, D. Gresch, Z. Wang, Q. Wu, M. Troyer, X. Dai, and B. A. Bernevig, *Nature (London)* **527**, 495 (2015).
- [42] J. Ruan, S.-K. Jian, D. Zhang, H. Yao, H. Zhang, S.-C. Zhang, and D. Xing, *Phys. Rev. Lett.* **116**, 226801 (2016).
- [43] G. Autès, D. Gresch, M. Troyer, A. A. Soluyanov, and O. V. Yazyev, *Phys. Rev. Lett.* **117**, 066402 (2016).
- [44] Z. Zhu, G. W. Winkler, Q. S. Wu, J. Li, and A. A. Soluyanov, *Phys. Rev. X* **6**, 031003 (2016).
- [45] J. Wang, X. Sui, W. Shi, J. Pan, S. Zhang, F. Liu, S.-H. Wei, Q. Yan, and B. Huang, *Phys. Rev. Lett.* **119**, 256402 (2017).
- [46] G. Chang, S.-Y. Xu, H. Zheng, B. Singh, C.-H. Hsu, G. Bian, N. Alidoust, I. Belopolski, D. S. Sanchez, S. Zhang *et al.*, *Sci. Rep.* **6**, 38839 (2016).
- [47] Z. Wang, M. G. Vergniory, S. Kushwaha, M. Hirschberger, E. V. Chulkov, A. Ernst, N. P. Ong, R. J. Cava, and B. A. Bernevig, *Phys. Rev. Lett.* **117**, 236401 (2016).
- [48] J.-W. Rhim and Y. B. Kim, *Phys. Rev. B* **92**, 045126 (2015).
- [49] Y. Huh, E.-G. Moon, and Y. B. Kim, *Phys. Rev. B* **93**, 035138 (2016).
- [50] M. Hepworth, K. Jack, R. Peacock, and G. Westland, *Acta Crystallogr.* **10**, 63 (1957).
- [51] B. G. Müller and M. Serafin, *Z. Naturforsch. B* **42**, 1102 (1987).
- [52] H. Effenberger, K. Mereiter, and J. Zemann, *Z. Kristallogr.* **156**, 233 (1981).
- [53] M. Huber and H. Deiseroth, *Z. Kristallogr.* **210**, 685 (1995).
- [54] L. Moreno, J. Valencia, D. L. Téllez, M. Martínez, J. Roa-Rojas, F. Fajardo, *J. Magn. Magn. Mater.* **320**, e19 (2008).
- [55] J. L. Garcia-Munoz, J. Rodriguez-Carvajal, P. Lacorre, and J. B. Torrance, *Phys. Rev. B* **46**, 4414 (1992).
- [56] See Supplemental Material at <http://link.aps.org/supplemental/10.1103/PhysRevLett.124.016402>, which includes Refs. [50–55, 57–67], for the computational methods, a symmetry operator analysis, the tight-binding model, and supplementary figures for the candidates.
- [57] G.-B. Liu, W.-Y. Shan, Y. Yao, W. Yao, and D. Xiao, *Phys. Rev. B* **88**, 085433 (2013).
- [58] H. Huang, J. Liu, D. Vanderbilt, and W. Duan, *Phys. Rev. B* **93**, 201114(R) (2016).
- [59] J. P. Perdew, K. Burke, and M. Ernzerhof, *Phys. Rev. Lett.* **77**, 3865 (1996).
- [60] P. E. Blöchl, *Phys. Rev. B* **50**, 17953 (1994).
- [61] H. Peng, Z.-H. Yang, J. P. Perdew, and J. Sun, *Phys. Rev. X* **6**, 041005 (2016).
- [62] V. I. Anisimov, J. Zaanen, and O. K. Andersen, *Phys. Rev. B* **44**, 943 (1991).
- [63] A. A. Mostofi, J. R. Yates, Y.-S. Lee, I. Souza, D. Vanderbilt, and N. Marzari, *Comput. Phys. Commun.* **178**, 685 (2008).
- [64] Q. Wu, S. Zhang, H.-F. Song, M. Troyer, and A. A. Soluyanov, *Comput. Phys. Commun.* **224**, 405 (2018).
- [65] Z. Wang, A. Alexandradinata, R. J. Cava, and B. A. Bernevig, *Nature (London)* **532**, 189 (2016).
- [66] S. M. Young and C. L. Kane, *Phys. Rev. Lett.* **115**, 126803 (2015).
- [67] R. Takahashi, M. Hirayama, and S. Murakami, *Phys. Rev. B* **96**, 155206 (2017).
- [68] A. Jain, S. P. Ong, G. Hautier, W. Chen, W. D. Richards, S. Dacek, S. Cholia, D. Gunter, D. Skinner, G. Ceder *et al.*, *APL Mater.* **1**, 011002 (2013).
- [69] L. Fu, *Phys. Rev. Lett.* **106**, 106802 (2011).
- [70] S. M. Young and C. L. Kane, *Phys. Rev. Lett.* **115**, 126803 (2015).
- [71] D. Gresch, Q. S. Wu, G. W. Winkler, R. Häuselmann, M. Troyer, and A. A. Soluyanov, *Phys. Rev. Mater.* **2**, 103805 (2018).
- [72] S. V. Halilov, A. Y. Perlov, P. M. Oppeneer, A. N. Yaresko, and V. N. Antonov, *Phys. Rev. B* **57**, 9557 (1998).
- [73] N. B. Kopnin, T. T. Heikkilä, and G. E. Volovik, *Phys. Rev. B* **83**, 220503(R) (2011).
- [74] G. Volovik, *Phys. Scr.* **T164**, 014014 (2015).
- [75] T. T. Heikkilä and G. E. Volovik, in *Basic Physics of Functionalized Graphite*, edited by P. D. Esquinazi (Springer, New York, 2016), pp. 123–143.
- [76] G. Chang, S.-Y. Xu, X. Zhou, S.-M. Huang, B. Singh, B. Wang, I. Belopolski, J. Yin, S. Zhang, A. Bansil *et al.*, *Phys. Rev. Lett.* **119**, 156401 (2017).
- [77] Q. Xu, E. Liu, W. Shi, L. Muechler, J. Gayles, C. Felser, and Y. Sun, *Phys. Rev. B* **97**, 235416 (2018).
- [78] J. Noky, Q. Xu, C. Felser, and Y. Sun, *Phys. Rev. B* **99**, 165117 (2019).
- [79] I. Belopolski, K. Manna, D. S. Sanchez, G. Chang, B. Ernst, J. Yin, S. S. Zhang, T. Cochran, N. Shumiya, H. Zheng *et al.*, *Science* **365**, 1278 (2019).
- [80] D. Liu, A. Liang, E. Liu, Q. Xu, Y. Li, C. Chen, D. Pei, W. Shi, S. Mo, P. Dudin *et al.*, *Science* **365**, 1282 (2019).
- [81] N. Morali, R. Batabyal, P. K. Nag, E. Liu, Q. Xu, Y. Sun, B. Yan, C. Felser, N. Avraham, and H. Beidenkopf, *Science* **365**, 1286 (2019).
- [82] H. Chen, W. Zhu, D. Xiao, and Z. Zhang, *Phys. Rev. Lett.* **107**, 056804 (2011).
- [83] C. R. Rajamathi, U. Gupta, N. Kumar, H. Yang, Y. Sun, V. Süß, C. Shekhar, M. Schmidt, H. Blumtritt, P. Werner *et al.*, *Adv. Mater.* **29**, 1606202 (2017).
- [84] J. Li, H. Ma, Q. Xie, S. Feng, S. Ullah, R. Li, J. Dong, D. Li, Y. Li, and X.-Q. Chen, *Sci. China Mater.* **61**, 23 (2018).